STABILITY OF NECKLACE BEAMS AND FEMTOSECOND FILAMENTATION IN WATER WITH IMPURITIES

A Thesis

Presented to the Faculty of the Graduate School

of Cornell University

in Partial Fulfillment of the Requirements for the Degree of

Master of Science

by

Daiwei Zhu

May 2015

ABSTRACT

This thesis presents two projects that investigate the nolinear pulse propagation in Kerr media. In the first project, the stability of necklace beams is experimentally and numerically studied. The effects of the size of bead in necklace beams on the propagation are examined. It is also found that the stable propagation of necklace beams is sensitive to the noise of the total bead energy among different beads, but it can tolerate a high level of random noise. In the second project, white light generation in water with impurities is experimentally investigated. White light generation from tap water and distilled water shows almost no difference. This agrees with that the avalanche ionization plays a much less important role in femtosecond filamentation than in optical breakdown. White light generation from distilled water and water-methanol mixture (2% methanol) is also measured, and no observable difference was found. This likely indicates that the ionization rates of water and methanol are similar, although their band gaps differ by more than 1 eV.

BIOGRAPHICAL SKETCH

Daiwei Zhu was born in Changsha, Hunan, P. R. China on October 17, 1990. He received a B.S. degree in Physics from the Wuhan University at Wuhan, P. R. China, in 2013. In August that year, he enrolled in the M.S. program in applied physics at Cornell University in Ithaca, New York, USA. From summer of 2014 till his graduation in 2015, he worked in the research group of Dr. Alexander L. Gaeta studying the dynamics of intense femtosecond pulses.

This thesis is dedicated to my parents Zhaofu Zhu and Yuling Li.

ACKNOWLEDGEMENTS

I would first like to thank Professor Alex Gaeta for allowing me to work on my master project in his research group. The guidance and insightful suggestions he has offered me are invaluable. The knowledge and experience I obtained under his instruction will greatly benefit my future career.

I would also like to thank my friends and colleagues Prathamesh Donvalkar, Mengjie Yu, and Gauri Patwardhan. The discussion I had with them inspired me a lot.

To Xiaohui Gao, who instructed me all along through my project, I would like to thank you for having been generously sharing your skills and knowledge in experiments, numerical simulation, and machining work with me.

To all the members of Gaeta Lab and my friends in AEP M.S. program, I really enjoyed working and having fun with you. The past year in Ithaca cannot be so colorful without you.

Finally, I would like to thank my parents Zhaofu Zhu and Yuling Li for their patience and care. Their support is what helped me overcome all the difficulties.

TABLE OF CONTENTS

LIST OF FIGURES

CHAPTER 1

INTRODUCTION

1.1 History of Filamentation

It had been long believed that ultrashort pulses can only propagate for a limited distance without significant attenuation of intensity, due to dffraction and group velocity dispersion. Considering a pulse with initial beam waist of 5 mm and initial pulse duration of 30 fs, after propagation in air for 1 km, its intensity will be attenuated by a factor of 5×10^3 due to dispersion and diffraction. But in nonlinear regime, when the pulse is ultra intense(Gw), the propagation can be very different. The propagation of intense ultrashort pulse for extended distance without external guiding is called filamentation or self-guided propagation. This phenomenon was first discovered by Braun *et al*. in 1995 [2]. In their experiment, a pulse of 775 nm, 200 fs and 15 mJ initial pulse energy had its intensity increased instead of decreased after long distance propagation. At the position of 10 meters away from the laser output, the intensity was so strong that air was ionized into bright plasma channel, which lasted for 20 meters long. Now, self-guided propagation as long as 2 km has been demonstrated [17].

Because of various potential applications, filamentation has been studied extensively since its first discovery. Many spectacular properties of filamentation have been discovered, together with applications based on them.

1.2 Formation of Filamentation

Filamentation is a complicated phenomenon that results from interplay of many physical effects such as diffraction, dispersion, Kerr effect, self-phase modulation, photo-ionization, plasma defocusing, and so on. But the origin of filamentation can be qualitatively understood with a simplified description given in this section.

Because of diffraction, the beam size increases as it propagates. For example, for Gaussian beams, the full width at half maximum (FWHM) will increase by a factor of $\sqrt{2}$ after it propagates over a typical length called Rayleigh length:

$$L_{DF} = \frac{k\omega_0^2}{2} = \frac{\pi n_0 \omega_0^2}{\lambda}, \tag{1.1}$$

where,n_0 is the refractive index in vacuum. ω_0 is the angular frequency of the light. λ is the wavelength of light. In normal dispersive media, light of higher frequency travels faster than light of lower frequency. So a pulse, containing different frequency component, also undergo temporal broadening as it propagates in media. This effect, called the group velocity dispersion, is characterized by the dispersion length:

$$L_{GVD} = \frac{t_P^2}{2k''}, \tag{1.2}$$

where t_P is the pulse duration and k'' is the second order derivative of wave vector with respect to angular frequency. For example, a pulse of initial duration $t_p = 10$ fs and central wavelength at 800 nm will increase its duration by 40% after propagation in air for 2.5 m.

In linear regime, the diffraction and the dispersion broaden the pulse (spatially and temporally) so that its intensity is attenuated as it propagates.

When the power of the pulse is high, nonlinear effects start to play significant roles. The Kerr effect is the intensity dependent refractive index. It results from the response of electronic polarization, molecular orientation, and other characteristics of the media to the intense electric field. Kerr effect can cause self focusing and self-steepening , thus compressing the pulse (spatially and temporally).

$$n = n_0 + n_2 I(r, t), \tag{1.3}$$

where n_0 is linear refractive index, $n_2 I$ is the intensity dependent refractive index and n_2 is proportional to $\chi^{(3)}$, the third order nonlinear susceptibility. If n_2 is a positive value, the higher the intensity is, the higher the refractive index will be. So for a beam with Gaussian(or similar) intensity profile, the refractive index is higher at center and lower at the edge. Thus the media act as a virtual convex lens that act against diffraction.The effect of self focusing depends on the intensity of the pulse at each point. And intensity of beam at different point is correlated. So the effect of self focusing is actually characterized by the critical power P_c. Different beam profiles usually has different critical power, of the same form [1]:

$$P_c = C\frac{\lambda_0^2}{n_0 n_2}. \tag{1.4}$$

The constant C depends on the exact profile, which is 0.2 for a Gaussian beam. Using data from [1], the critical power P_c in air of beam with 800 nm wavelength is calculated to be about 3GW. If the power of the beam exceeds P_c,

the self-focusing overcomes diffraction that the size of the beam decreases as it propagates until collapse, as shown in Fig.1.1(a). If the power is smaller than P_c, the beam diffracts.

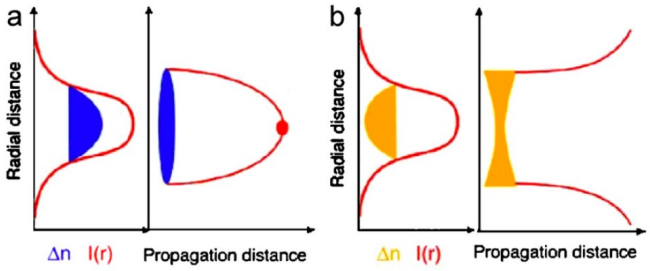

Figure 1.1: (a) Self focusing caused by Kerr effect. The graph illustrates the refractive index dependence on the intensity of the beam and how it acts as a lens that converges the beam when its power exceeds P_c. (b) Similar case that the plasma defocuses the beam. This actually acts like an Kerr effect with $n_2 < 0$. (Adapted from Ref.[5])

The collapse of beam with initial power $P > P_c$ happens when the beam is focused to the point that its intensity is high enough to generate plasma. Two major processes through which the beam generates plasma are multiphoton ionization and avalanche ionization. In the case of ultrashort pulses, the ionization is mostly caused by multiphoton ionization.The presence of plasma will result in a reduction of local refractive index, which is described by the following equation [9]:

$$n \simeq n_0 - \frac{\rho(r,t)}{2\rho_c}, \tag{1.5}$$

where $\rho(r,t)$ is the plasma density and ρ_c is the critical density at which the medium becomes opaque. The rate of multiphoton absorption is proportional to I^k. Here I is the intensity and k is the number of simultaneously absorbed photons through ionization (for 800 nm light, $k = 8$). So, the local plasma density

$\rho(r,t)$ increase as I increases, resulting in a lower refractive index. Following the same reasoning of self focusing, the plasma also acts as a virtual concave lens. So the beam is defocused, as shown in Fig.1.1 (b). Because the reduction of refractive index is dependent on I^k and I increases abruptly through the collapse, the plasma defocusing is also an abrupt process.

Under the interplay of the effect discussed above, it can be qualitative seen that the light beam will undergoes cycles of focusing and defocusing, as shown in Fig.1.2.

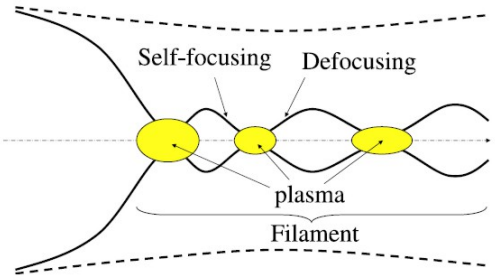

Figure 1.2: Schematic representation of the focusing-defocusing cycles of the light . The solid curves indicate the diameter of the intense core of the light. The filamentation length is the distance covered by these cycles. The dashed lines indicate the root mean square radius of the full beam. Note that the actual gap between plasma clusters is very small, though it seems big in this graph. (Adapted from Ref.[5])

1.3 Properties of Filamentation

Filamentation is accompanied with many spectacular properties that are of great potential in practical applications. Brief introductions of several properties that are relevant to my projects are given in this section.

1.3.1 Long Range Propagation

The most important aspect of filamentation is its ability to maintain the intensity over a long distance. In the experiment [18], the peak intensity of pulse can stay as high as 10^{12} W/cm^2 for several kilometers. The termination of filamentation is mainly caused by the energy loss of ionization. Because of the plasma defocusing, the peak intensity is clamped around the threshold of multiphoton absorption. The short duration of femtosecond pulses minimized the avalanche ionization process. So the energy loss is minimized for filamentation. For many laser related sensing technology like laser induced breakdown spectroscopy, high intensity over a long distance is required, which could be achieved by filamentation.

1.3.2 Self Cleanning

The filamentation is inherently a nonlinear process. In many nonlinear systems, states with different initial conditions evolves into same states (attractors). Filamentation also shows similar behavior. If a beam's initial peak power is greater than the P_c, it will collapse and then undergo several focusing and defocusing cycles as described above. Through this process, the pulse always evolves into a special profile called Townes profile [4]. This process has been observed by different group before[20, 21]. Even the peak power of pulse is smaller than P_c, it still show tendency to develop into Townes profiles but overwhelmed by diffraction. This properties is not only of fundamental interest, but can also be used to manipulate the spatial profile of pulse, like cleaning the noise of the pulse before it goes into some noise sensitive process.

1.3.3 Plasma Channel Formation

As described above, filamentation is accompanied with significant ionization. When the intensity pulse passes through media, it ionizes the media and leaves a plasma channel behind. The free electron density along the trajectory of filamentation is usually measured to be the order of 10^{16} cm^{-3} [5]. The lifetime of the generated free electron is usually about 100 ns [26]. Under special condition, the lifetime can go above one micro second [26].

Because of conducting property of plasma, the filamentation is thought to be a potential way of generating conducting channel remotely. Guiding of lightning with filamentation have already been demonstrated [25]. Using this plasma channels as waveguides is also demonstrated [8].

In gases, the ultra intense pulse dissociates the molecules along its trajectory and excites the dissociated atoms into excited states. The excited atoms along the trajectory then work as gain media and generate backward lasing [6].

1.3.4 Supercontinuum Generation

When a ultrashort pulse propagates in a medium, because of the nonlinear effect, its spectrum will get significantly broadened. This is called supercontinuum generation, or white light generation, as significant white light can be seen along the trajectory in experiment. Various mechanisms can cause the generation of white light. For ultrashort pulses, the major mechanism that causes the supercontinuum generation is self phase modulation (SPM).

It's illustrated in previous section that in Kerr media, the refractive index

depends on intensity as shown in Eq.1.3. So an approximation of the frequency of the pulse at each time can be expressed as follow:

$$\omega(t) = -\frac{\partial \phi}{\partial t} \approx \omega_0 - \frac{n_2 \omega_0}{c} z \frac{\partial I(t)}{\partial t}. \tag{1.6}$$

It can be read from the equation that new frequency will be generated from the second term on the right side of Eq.1.6. Because $\frac{\partial I(t)}{\partial t} > 0$ at the leading part of the pulse, it generates lower frequency component. Because $\frac{\partial I(t)}{\partial t} < 0$ at the tailing part of the pulse, it generates higher frequency component.

This can also be viewed from another perspective. Because of Kerr effect, the refractive index is higher for the peak than it is for the front and tail of the pulse. So the peak of the pulse moves slower than the front and the tail. This shifts the peak away from the front to the tail. So the front of pulse is stretched: it becomes redder. The tail is compressed: it becomes bluer. The temporal reshape of the pulse from this effect is called self steepening, as part of the pulse is compressed so the peak become sharper. As sharper temporal profile correspond to broader spectrum, the self steepening directly corresponds to the supercontinuum generation.

Supercontinum generation generates directional coherent white light. So it can be used in various application such as remote detection and spectroscopy.

1.3.5 Multiple Filamentation

When the initial peak power P_0 of a pulse is significant higher than the critical power P_c, the modulation instability of the pulse (imperfection or asymmetry)

will cause the pulse to split into certain amount($\sim \frac{P_0}{P_c}$) of separate filaments propagating in parallel direction. This is called multiple filamentation.

In general, the distance where the pulse breakup depends on the extent of modulation instability. Pulses with smaller instability breakup at a longer distance. The onset of multiple filamentation also depends on the peak power of the initial pulse. When the initial peak power is much greater than critical power($P_0 \sim 100P_c$), small spatial imperfection can be amplified through nonlinear interaction and cause the beam to break up into multiple filaments at a distance$\sim 1/P_0$, before the pulse collapses [10]. Pulse with smaller initial peak power will first collapse at distance$\sim 1/\sqrt{P_0}$ and then break up into multiple filaments.

For big modulation instability, the profile of the pulse after multiple filamentation is well predictable. But in the case where small perturbations amplified through nonlinear interaction, like multiphoton absorption, the profile after multiple filamentation is pretty chaotic. It can be viewed as the sensitivity of the dynamics of the nonlinear propagation to the initial condition.

CHAPTER 2

STABILITY OF NECKLACE BEAMS

2.1 Pre-collapse Behavior of Femtosecond Pulses

If the self-focusing keep increasing the intensity of the beam, higher order nonlinear effect, such as plasma defocussing, will starts to play a significant role. Then the beam is considered collapsed. The propagation of beam before collapse is usually called pre-collapse regime. The complex propagation after collapse is usually referred to as post-collapse regime. Pre-collapse regime of femtosecond pulses is of great interests for several reasons.

First, the collapse process corresponds to a catastrophic increase in the peak intensity of the pulse. For most solid media, such catastrophic increase of intensity could result in permanent damage. Restricting the pulse propagation to the pre-collapse regime can lower the probability of medium damage. Second, even in gas or liquid, the energy loss through ionization after collapse is the main factor that terminates the filamentation. The rate of loss increases as the peak intensity increases. So, one cannot effectively increase the filamentation length by simply contain more energy into the pulse. Moreover, because the collapse is a process with high nonlinearity, it is very sensitive to initial condition of the pulse. In experiment, it is hard to have control over the collapse dynamics.

So, in order to efficiently extend the propagation distance of femtosecond pulse, it is better to achieve stationary propagation in pre-collapse regime.

In the pre-collapse regime, the intensity is at the level that Kerr effect plays

significant roles but all the other higher order nonlinear effects are negligible. So, the proper description of the system only requires three effects: diffraction, group velocity dispersion, and Kerr effect. This can be expressed into nonlinear Schrödinger equation (NLSE)[11].In general, the NLSE has dimensionless form:

$$i\psi_z + \Delta\psi + \left|\psi^2\right|\psi = 0. \tag{2.1}$$

The ψ_z corresponds to the derivative of amplitude with respect to axial distance. The second Laplace operator included the second order derivative with respect to both temporal (dispersion) and transverse spatial (diffraction) coordinates. The stable propagation of optical pulse corresponds to soliton solutions of this equation.

2.2 Necklace Beams as Quasi-Solitons

Solitons are self-reinforced pulses that propagate in media without changing their spatial or temporal profile. The NLSE have stationary solutions. But these solutions have to be stable to be considered as solitons. The stability of the stationary solutions of NLSE depends on the dimension of the system.

To describe a wave with NLSE, one needs at least a 2-dimensional space(axial direction and a transverse direction). Only such 2D (like continue wave in planar dielectric waveguide) systems have stable stationary solutions [11]. These 2D soliton solutions can be analytically obtained through a technique called inverse scattering method.

For >2D system, there is no stable stationary solutions. Any solution that

have an infinitesimal deviation from the stationary solution will eventually either collapse or spread out. For example, in free space the continue wave beam have a stationary profile called Townes profile. Any beam deviated from it will approach it and collapse during the process[20].

In Ref. [23], necklace beams are proposed as "quasi-solitons": pulses that can maintain their spatial or temporal profile much better than normal pulse. Quasi-solitons still undergo spatial and temporal broadening due to diffraction, dispersion, or other effect. But the rate of broadening is very slow.

The origin of the idea that necklace beam could be a quasi-soliton is clear. A soliton solution of 2D NLSE has Sech(x) shape profile. Mathematically,the only difference in 3D NLSE is the one additional second order derivative term in the Laplace operator, say $\frac{\partial^2\psi}{\partial y^2}$. Thus, one would expect that a beam that is uniform in y direction can get rid of this term and becomes soliton. But $\frac{\partial^2\psi}{\partial y^2} = 0$ states are not stable in 3D NLSE. One way to overcome this instability is to periodically modulate the beam in y direction instead of make it uniform[16]. The modulated beam looks like a standing wave in y direction. Because of Kerr nonlinearity, those antinodes have higher refractive index. The result is that each section of the beam in y direction forms a virtual waveguide and overcomes the instability.But it is unpractical to generate an infinite long array in y direction. If we connect the head of the chain with the tail so that it forms a necklace shape (the y direction is changed into azimuthal direction), the chain becomes "infinity". The difference is that the chain now has a curvature. But if the radius of the necklace is much larger than the width of each section, this difference can be ignored. This necklace profile is described by Eq.2.2.

$$\psi(r, \theta, z = 0) = \alpha \text{sech}[(r - L)/W]\cos(\Omega\theta). \tag{2.2}$$

In Ref.[23], numerical simulation of the necklace beam is made. The result is shown in Fig.2.1.

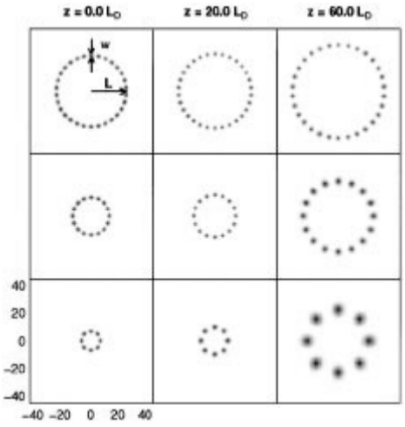

Figure 2.1: The numerical simulation result given in reference[23]. Different rows are results for necklace beams of different number of beads. Different column correspond to the profile of necklace beam after propagated for z distance. $L_D = 2\pi n W_0^2/\lambda$ is the diffraction length defined with respect to a single bead.

2.3 Experimental Generation of Necklace Beams

The experimental observation of necklace beam has been done by members of Gaeta Group before [15]. According to Ref. [15] , the necklace beam , although having better stability, still suffers from significant spatial broadening. The first idea I had is by increasing the number of lobes in the necklace beam, the stability can be enhanced.

One of the most important parts of the experiment is the generation of the

necklace beam. First, it is hard to produce the exact profile described by Eq. 2.2. So, a close choice will be the well-known Laguerre-Gaussian (LG) TEM_{pl} modes. These modes also have similar necklace shape profile. It is expected that if the exact necklace beams are quasi-solitons, then the similar LG modes should also exhibit higher stability. The setup used to generate the LG beam is shown in Fig. 2.2. Second, the necklace beam discussed above is a continuous wave. But in experiment, to achieve enough intensity(nonlinearity), ultrashort pulse is the only possible choice. The ultrashort pulse propagation in 3D space actually corresponds to the 4D NLSE. Still, the idea here is that if the continuous wave necklace beam exhibits higher than usual stability, so should the femtosecond pulse necklace beam. Also, as shown later, simulation of 3D NLSE is in good qualitative agreement with experiment.

The light first go through a combination of a polarizer and a half-wave plate so that its intensity can be adjusted. Then the pulse passes through a spatial filter made up of two lens and a pin hole so that the higher spatial frequency component of the pulse can be cleaned. This first spatial filter is set in vacuum environment, because, at this stage, the intensity of the pulse is high that nonlinear effect can play a significant role. After the spatial filter, the pulse will approximately have the lowest mode Gaussian spatial profile, so it can evenly and symmetrically incident on the 16-sections phase plate. Each sections of the phase plate has π phase difference with its neighborsone . The phase plate changes the profile of the pulse into a combination of many higher order Gaussian modes, in which the most significant component is the Gaussian mode that has 16 section ringed in a circle. Next, the pulse passes through the second spatial filter so that all high order Gaussian mode except the desired one are filtered out. The pulse then passes through a beam splitter so that the pulse energy is

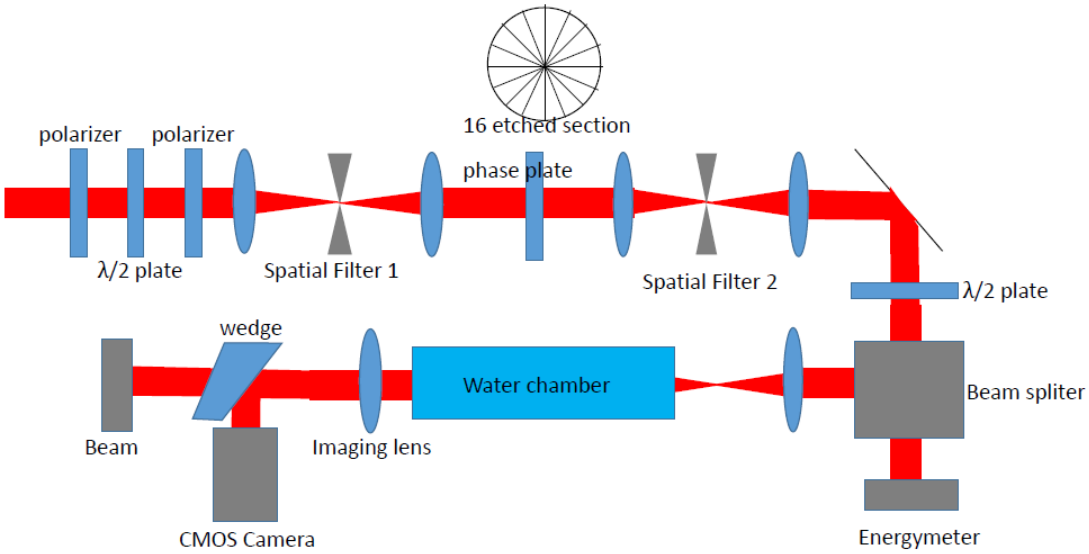

Figure 2.2: Sketch of the setup used to generate necklace shape beam. The light is turned into high order LG mode after passing through the 16-sections etched phase plate. The effect of non-linear effect is studied by compare the profile before and after propagate through the water chamber at different energy(peak power).The propagation of the pulse outside the water chamber is assumed to be linear as the peak power of pulse is much lower than the P_c in air.

monitored by the energymeter. The ratio of the beam splitter depends on the polarization of incident light, so the proportion of monitored energy can be adjusted. The pulse then enters the water chamber and undergoes Kerr effect. A lens is used to image the output surface of the chamber onto the sensor of the CMOS camera.

In order to study the stability of the LG beam, the profiles of the pulse before and after it passing through the water chamber are compared. The nonlinearity of the propagation is controlled by adjust the power of the input pulse. The result is shown in Fig.2.3.

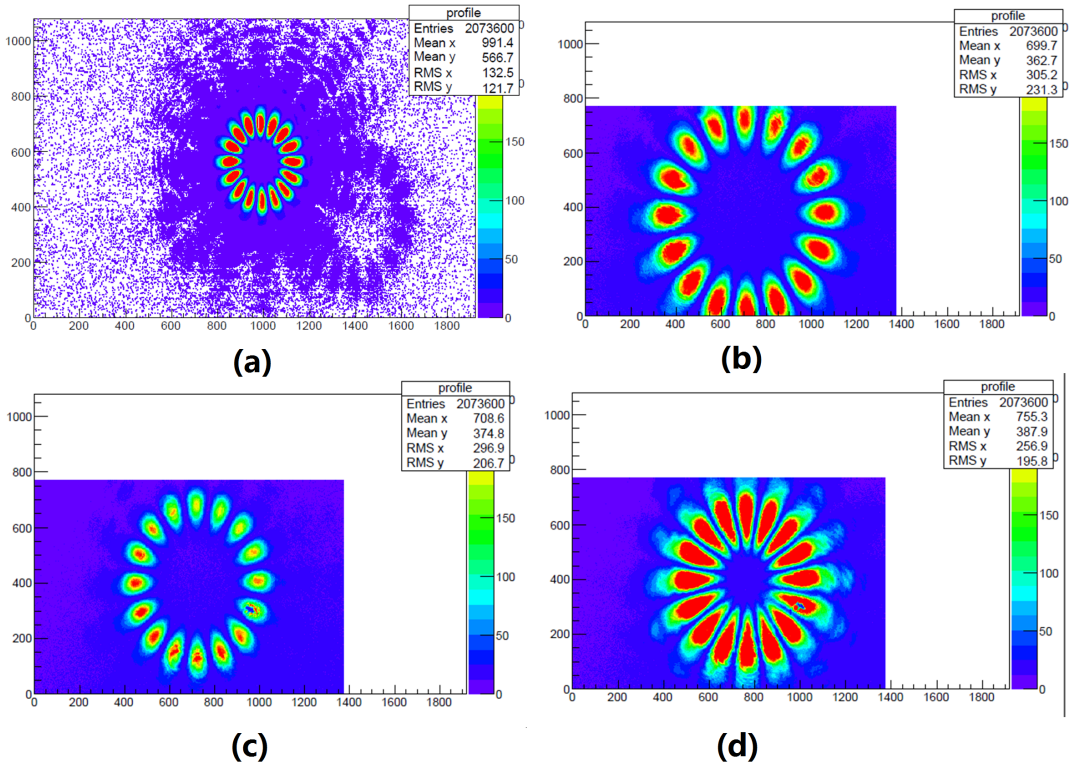

Figure 2.3: The comparison of LG mode beam propagate through the water chamber at different nonlinearity(different pulse energy). (a) is the initial profile of the pulse, measured at the entrance of the chamber, with light directly incident on the sensor of the CMOS camera. (b) profile of the pulse at the output plane of the chamber, with no nonlinearity (waterchamber removed). (c)profile of the pulse at the output plane of the chamber, with weak nonlinearity (P_{peak} ~ 15MW). (d) profile of the pulse at the output plane of the chamber, with strong nonlinearity (P_{peak} ~ 75MW). Because (b),(c) and (d) are captured by using a lens to image the water chamber's output plane onto the CCD's sensor, it is rescaled to match that of (a). Because of saturation of the CMOS camera at high input intensity, (d) lost part of the information about the peak intensity distribution.

Comparing Fig.2.3.(c) with Fig.2.3.(b) we can found that the nonlinearity does limited the broadening of the LG beam. Due to nonlinear effect, at same distance, both radius of each individual bead and the radius of the whole ring is

smaller than that in the linear propagation condition. Figure.2.3.(d) corresponds to higher nonlinearity. We should observe smaller individual bead width and smaller whole ring radius. However, in (d) it looks like though the radius of the whole ring is smaller than (c), each bead is stretched along radial direction. This is caused by saturation of CMOS camera.

The stability of LG mode did not reach the extent proposed in Ref.[23]. The difference between LG modes and necklace beam is probably more significant than the expectation.

2.4 Numerical Simulation of NLSE

In the pre-collapse regime, NLSE have already included all the significant effects.In my simulation, I ignored the dispersion term in the Laplace operator in NLSE. Mostly, this greatly increased the efficiency of the simulation, as the time dimension is ignored. Second, the qualitative agreement between my simulation and experimental measurement turns out to be outstanding. The attenuation of intensity (nonlinearity) seems to be equivalent to the shortening of the nonlinear media.

The exact form of NLSE used in my simulation is shown in Eq.2.3

$$i\psi_{\zeta} + \frac{1}{4}(\psi_{\mu\mu} + \psi_{\nu\nu}) + \frac{L_{df}}{L_{nl}}\left|\psi^2\right|\psi = 0. \tag{2.3}$$

The amplitude of ψ is normalized. $\zeta = z/L_{df}$, $\mu = x/r_0$,$\nu = y/r_0$, $L_{df} = \frac{\pi n_0 r_0^2}{\lambda}$ is the standard diffraction length of a Gaussian beam of waist width r_0. So the

length in this equation is normalized with respect to a Gaussian Beam. $L_{nl} = \frac{\lambda}{2\pi n_2 I}$ is the nonlinear length.

The numerical integration is done with split step scheme. The term $\frac{1}{4}(\psi_{\mu\mu} + \psi_{\nu\nu})$ is integrated with Fourier transformation. The term $\frac{L_{df}}{L_{nl}}\left|\psi^2\right|\psi$ is integrated with second order Runge-Kutta method.

First, whether the simulation matches the experiment is checked. The result is shown in Fig.2.4.

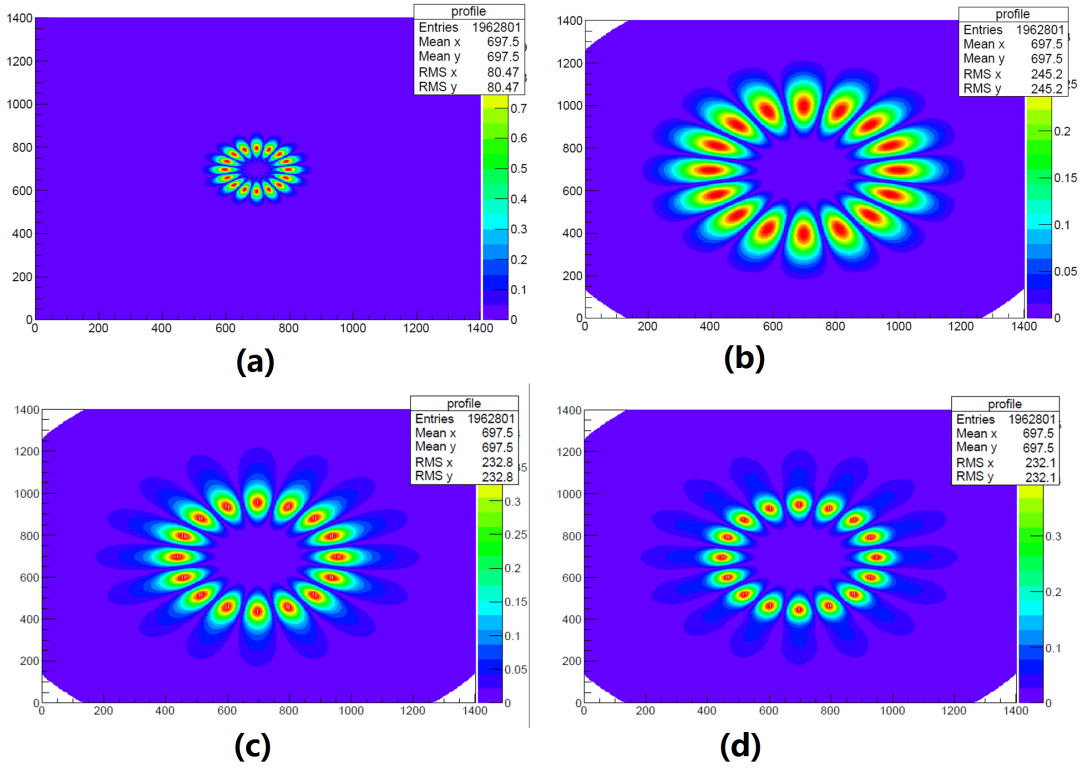

Figure 2.4: Initial input profile and the simulation result of Eq.2.3 with different L_{nl}. (a) is the initial profile of the necklace beam (b) profile of the beam after propagation without nonlinearity. (c)is the profile of the beam propagated with weak nonlinearity. (d) is the profile of the beam propagated with strong nonlinearity.(a) (d) each correspond to the experimental result in fig2.3.

The simulation results are in good agreement with the experiment measurement. Recall that extra broadening in Fig.2.3(d) is caused by saturation of CMOS camera. We can see in Fig.2.3(d) that if the graph is saturated at about 0.1, it will match the Fig.2.3(d) well.

From the simulation result, the stability of LG mode is still not significant.

It is known that the diffraction length of higher order LG mode does not directly correspond to the width of each individual lobe, but the array of lobes as a whole. In other words, if the size of individual lobe is the same, the diffraction length of a higher order LG mode is longer than that of a lower order mode. But in Ref.[23], the diffraction length is defined with respect to the individual bead of the necklace beam W. The more realistic measure of the broadening should be based on the diffraction length defined with respect to the radius of the whole necklace beam L. This is illustrated in Fig.2.5. In this case, even without nonlinearity, the broadening is negligible after propagating for $3L_{df}$, which is defined with respect to the width of individual bead W. But if it is defined with respect to the radius of the necklace as a whole L, it is only $0.3L_{df}$.

2.5 Effects of Individual Lobe Size W.

Another factor that may result in lower stability is the difference between a necklace beam described by Eq.2.2 and the LG mode. Comparing Fig.2.4 with Fig.2.3, it is clear that LG mode is similar to necklace beam with $w/L = 3/10$. But in [23], this ratio is smaller. It is important to study how this ratio affects the stability of the necklace beam.

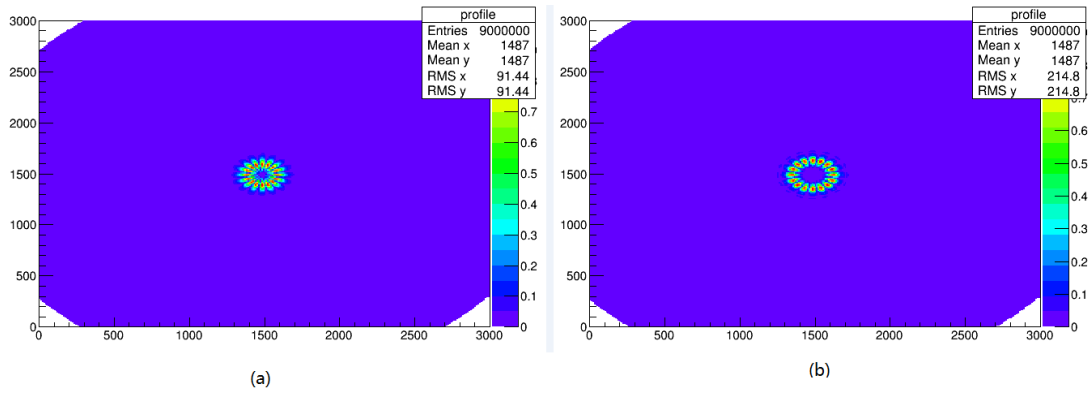

Figure 2.5: The linear propagation of necklace beam. (a) Initial profile.(b) profile after propagate for $z = 3L_{df}$. L_{df} is defined with respect to W, the width of individual bead.

Necklace beams with $L = 1$ and W ranging from 0.08 to 0.5 is numerically simulated at various nonlinearity.

First, this ratio W/L approximately corresponds to the ellipticity of each individual bead. If this ratio is between 0.08 and 0.1, each individual bead is approximately round. If the ratio is smaller than this range, each bead is approximately an ellipse with major axis along azimuthal direction. If the ratio is greater than that range, each bead is approximately an ellipse with major axis along radial direction. This is illustrated in Fig.2.6

The effect of ellipticity is two folded. Nonlinearly, this ellipticity(asymmetry) acts as modulation stability and lead to multiple filamentation along the major axis. The ellipticity-induced multiple filamentation in a single Gaussian lobe case has been studied before[14]. An illustration of both the ellipticity induced multiple filamentation in our case and that in single lobe case[14] is shown in Fig.2.7. If we arrange an array of single lobe shown in Fig.2.7(b) into a circle, the multiple filamentation obtained will be similar to the case of Fig.2.7(a). It is

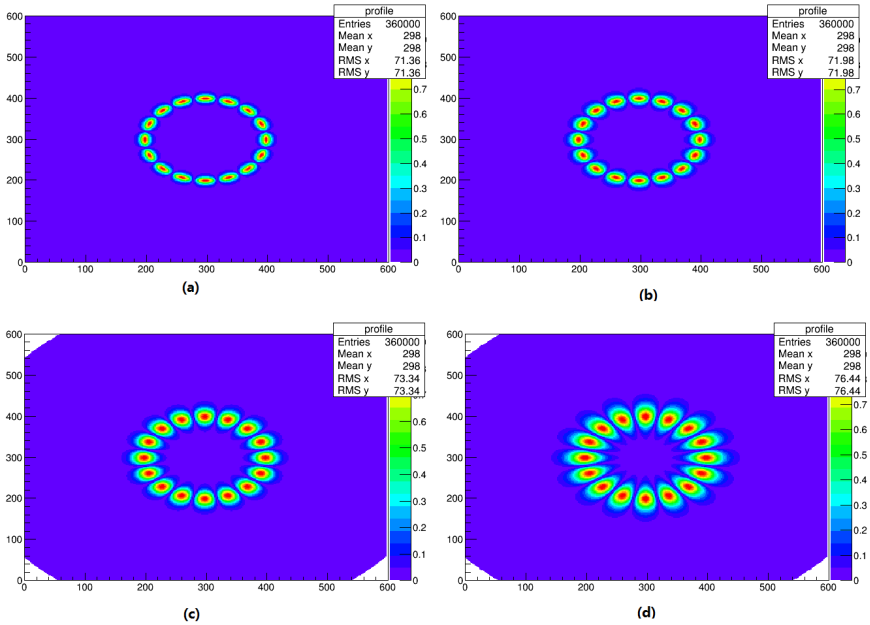

Figure 2.6: Necklace beam with same $L = 1$ but different W. (a)$W = 0.5$ (b)$W = 0.7$ (c)$W = 0.1$ (d) $W = 1.5$

worth mentioning that the multiple filamentation happens easier if the ellipticity become greater (lower threshold for multiple filamentation corresponds to bigger ellipticity).

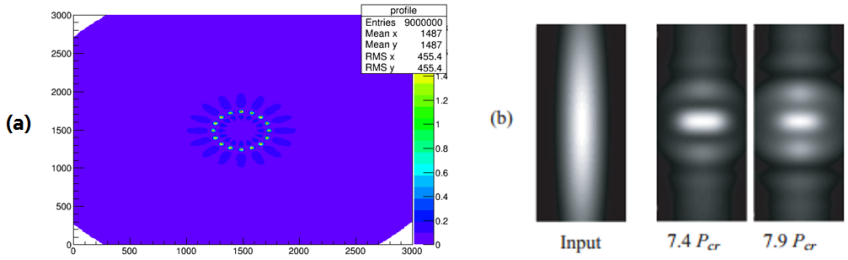

Figure 2.7: Multiple filamentation induced by ellipticity in both necklace beam case and single lobe case.(a) simulation result of $L = 1, W = 0.3$, at high nonlinearity(b) Simulation result given in Ref.[14] where ellipticity cause multiple filamentation of a single lobe.

Linearly, profiles deviated from LG mode will deform and generate diffrac-

tion pattern as they propagate. The LG mode used is similar to necklace beam with $W/L \approx 0.3$. So, the more this ratio deviated from 0.3, the stronger the diffraction will be.

Looking for beam with higher stability, defects like multiple filamentation and diffraction pattern should be avoid. The diffraction can be largely counteracted by Kerr nonlinearity, but the multiple filamentation always occurs when nonlinearity is above a threshold(depend on ellipticity). If the ratio of W/L is too small, the beam deviated from LG mode a lot. Thus high nonlinearity is needed to counteract the diffraction. But when W/L is too small, each lobe has a big ellipticity, nonlinearity cannot be high or multiple filamentation occur. From the simulation, I found that necklace beam with $W/L < 0.1$ cannot maintain its shape no matter what the nonlinearity is. For this reason, the best stability is expected to be achieved when $W/L \approx 0.1$, so each lobe is almost round.In this case, the threshold for multiple filamentation is highest, higher nonlinearity can be imposed to confine the diffraction. A comparison is shown in Fig.2.8.

The broadening of each beads in a necklace beam with $W = 0.1$ is obviously smaller than that of necklace beam with $W = 0.3$. The quantitative comparison of the expansion of the necklace ring as a whole and the attenuation of peak intensity in these two cases are also performed. The result is shown in Fig.2.9

Fig.2.9(a) shows that peak intensity attenuates slower for a necklace beam with $W = 0.1$. The difference is actually more significant if we notice that the ratio of initial max intensity in $W = 0.1$ case versus that of $W = 0.3$ case is $65 : 15$. Fig.2.9(b) shows that the expansion rate of the necklace ring as a whole is slower for $W = 0.1$ case. As the two line in Fig.2.9(b) have different slope, the difference will increase as they propagate.

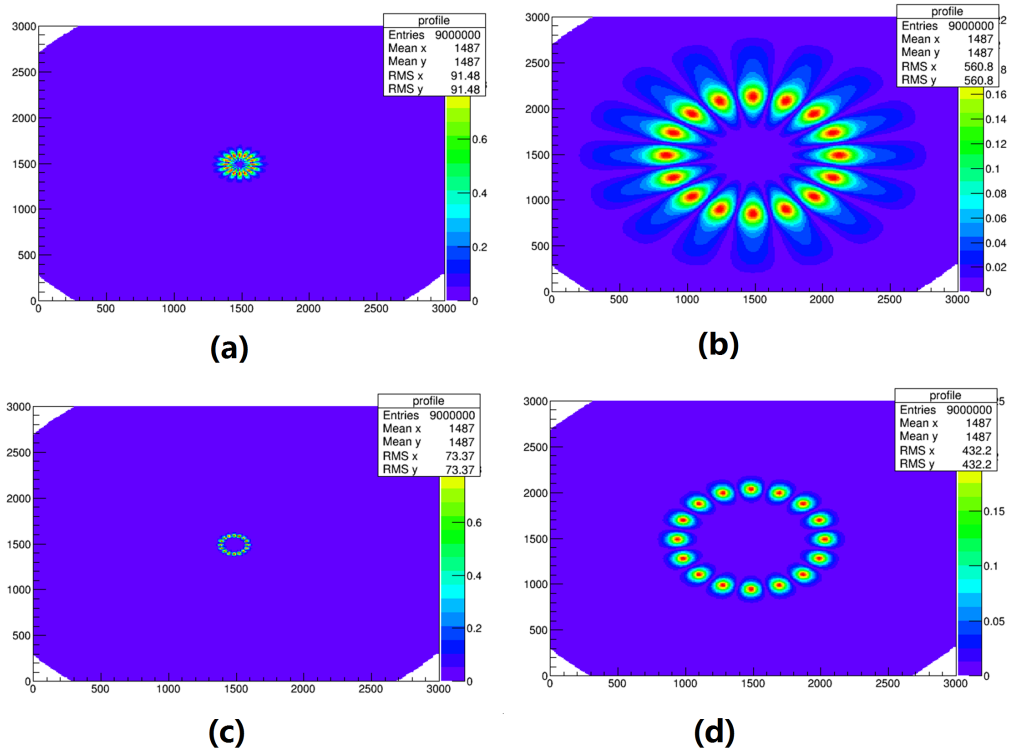

Figure 2.8: Comparison of the stability of necklace beam with different W.(a)necklace beam with $W = 0.3$ at $Z = 0$.(b)necklace beam with $W = 0.3$ at $Z = 2L_{df}$.(c)necklace beam with $W = 0.1$ at $Z = 0$.(d)necklace beam with $W = 0.3$ at $Z = 2L_{df}$. L_{df} here is defined with respect to the radius of the whole necklace ring L. The nonlinearity in each case is set at the highest value that deform like multiple filamentation does not occur. That is: in (a)and(b), $L_{nl}/L_{df} = 15$. In (c)and(d), $L_{nl}/L_{df} = 65$. Note this ratio is directly proportional to intensity.

2.6 How to Adjust the Lobe Size W

The size of individual lobe W can be adjusted by modification based on the setup shown in Fig.2.2. It can adjust the ratio W/L to value ranging from about 0.1 to about 0.3.

If the peak power of a beam is greater than P_c, it will collapse. For the neck-

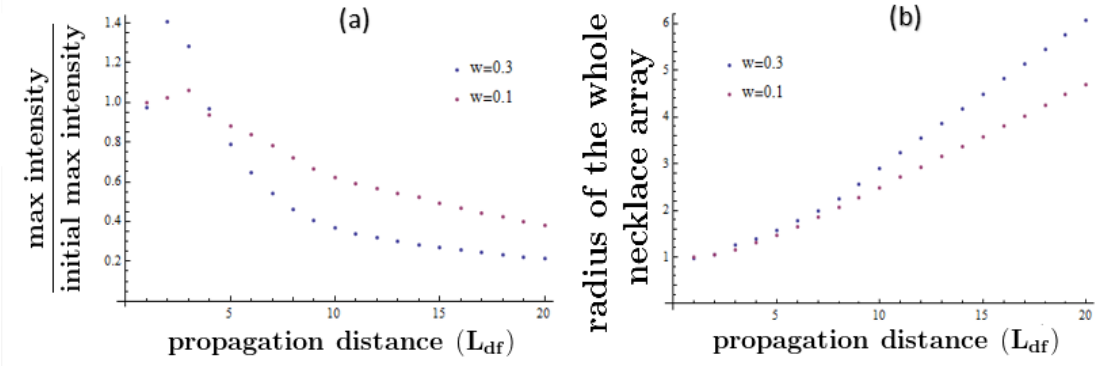

Figure 2.9: (a)Comparison of expansion of whole radius of the necklace beam$L$ with different W. (b)Comparison of attenuation of the peak intensity of the necklace beam with different W.

lace beam of n lobes, the critical power $P_c \approx nP_{c0}$ [15]. Here P_{c0} is the critical power of a lowest Gaussian mode beam and n is the number of lobes. The stability of necklace beam results from the coupling of each lobes. But when the $P > P_c$, lobes of the necklace beam will decouple from each other and collapse independently, approaching Townes profile[20].

The LG modes generated with my setup is similar to $W = 0.3$. An array of Townes profile corresponds to $W = 0.1$. So if the LG mode pulse has $P > P_c$, during its propagation, each bead will collapse and start to change W from 0.3 to 0.1. After W has reached the desired value, a ND filter can be used to attenuate the beam to recover the coupling.

Numerical tests of this approach is done by letting a necklace beam with $W = 0.3$ propagate with high nonlinearity. A demonstration is shown in Fig.2.10.

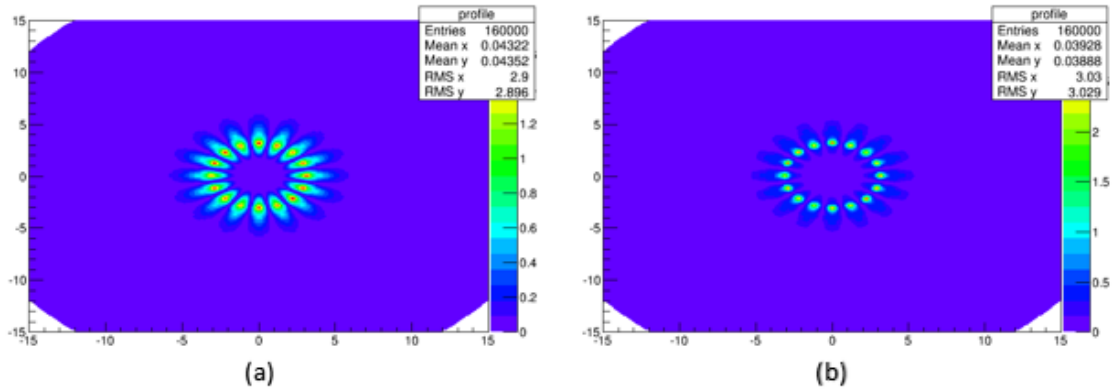

Figure 2.10: Numerical demonstration of how high nonlinearity decouples beads in the necklace beam and changing the W parameter. Initial profile has $W = 0.3$. $L_{nl}/L_{df} = 30$. (a) is at $z = 0.04L_{df}$. (b) is at $z = 0.08L_{df}$. In the simulation, 10% of noise is imposed.

2.7 Effect of Noise

Noise's impact on the stability of necklace beam is also studied numerically. Two types of noise are studied.

First type of noise is created by letting the intensity at each grid of the simulation window fluctuate for a certain level. It is like the usual background noise. The necklace beams are highly resistant to this type of noise. Noise level as high as 40% doesn't have significant impact on the dynamics. This can be explained by the self-cleaning effect.

However, the necklace beam is very sensitive to the second type of noise: the intensity of each lobe as a whole is fluctuated with a certain noise level. In other words, the brightness of each lobe is different by a little amount. In this case, noise level as low as 5% can break the stability of necklace beam. This is demonstrated in Fig.2.11.

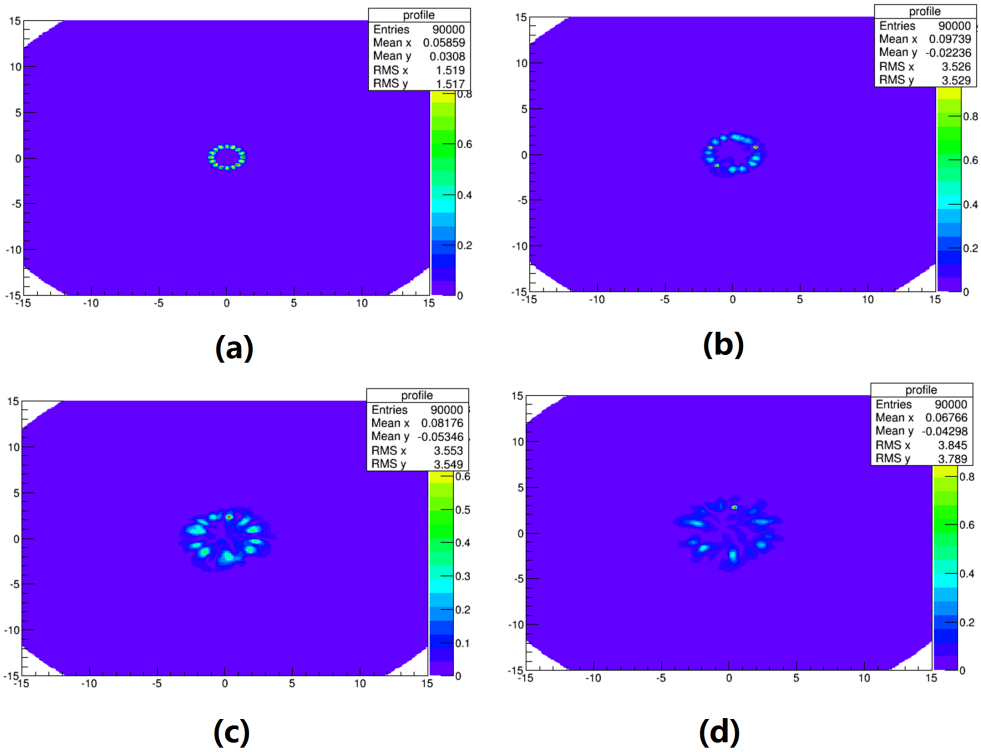

Figure 2.11: Evolution of Necklace beam with 5% noise. The noise is imposed so that the brightness of each lobes of the necklace array is different. In the simulation, $W = 0.1$ and $L = 1$. (a) profile at $z = 0.3L_{df}$. (b) profile at$z = 0.6L_{df}$. (c) profile at$z = 0.8L_{df}$.(d) profile at$z = 1L_{df}$.

The noise in experiment is actually the second type. After the first spatial filter in Fig.2.2, the profile is improved, but still not perfect. So the light cannot incident on the 16-sections phase plate evenly. Thus, the final LG profile will have the second type noise. It can be seen from Fig.2.3.

Although during the reshaping process this noise is negligible because lobes are decoupled, after coupling is recovered, the noise destroy the necklace array quickly.

2.8 Conclusion

The stability of necklace beam can be viewed in several several aspects.

First, the nonlinearity cannot significantly limit broadening of the radius of the whole necklace array. But the simulation does show that the increase of L is slower for necklace beam.

Second, the nonlinearity does have a significant contribution to the stability of each individual lobe(bead) of the necklace beam. The broadening of each lobe in a necklace beam is smaller than that of LG mode beam.

Thirdly, the maximum peak intensity necklace beam can have without breaking its shape is significantly higher than LG mode beam. The attenuation of peak intensity is slower for necklace beam.

Since the necklace beam is very sensitive to the noise of total bead energy among different beads, the stability numerically tested is hard to be demonstrated experimentally.

CHAPTER 3

FEMTOSECOND FILAMENTATION IN WATER WITH IMPURITIES

Ultraintense femtosecond pulses interact strongly with the media. One of the main result from the interaction is ionization. In gases or liquid, the plasma channel formed through ionization can be used as a conducting line or waveguide. In solid state media, permanent modification of physical properties of media through ionization can be used as a micromachining method [13]. Thus, study of how ionization affects the dynamics of femtosecond filamentation is of practical importance.

In femtosecond filamentation, ionization is mainly caused by two processes: multiphoton ionization and avalanche ionization. They correspond to two fundamental way that light field transfers energy to bound electrons.

Bound electrons can get energy from the light field by absorbing enough photons simultaneously so that it pays off the ionization energy and become a free electron with the rest kinetic energy. So, the smallest amount of photon absorbed simultaneously should equal the smallest integer K so that $Kh\nu \geqslant E_{gap}$. Here h is the Plank constant, E_{gap} is the band gap of the medium, and ν is the frequency of the light. For example, for the 800 nm light, the energy of a single photon is about 1.547 eV. The energy gap of distilled water is reported to be 7.5 eV [3]. So multiphoton ionization of distilled water is generally believed to be a five photon process. However, other values have also been reported [19].

With already existing free electrons, avalanche ionization is a process through which the electron population can be increased. The free electrons gain energy trough the inverse-bremsstrahlung absorption : the inverse of the pro-

cess that electrons emitting light after been scattered by ions. After the free electron's energy exceeds E_{gap}, it can knock out other bound electrons. So, as the name suggest, the number of free electrons increases in an avalanche manner. Because the inverse-bremsstrahlung absorption needs time to happen, its contribution decreases as the duration of incident light decreases.

The contribution of multiphoton ionization has long been confirmed. But how important the avalanche ionization is in the dynamics of femtosecond filamentation is still under debate. In Ref.[7, 12], the avalanche ionization is found to be the major source of free electrons in the trajectory of filamentation, while in some other literature [24], the avalanche ionization is thought to be negligible because of the ultrashort pulse duration.

In filamentation peak intensity is increased through self-focusing. With external focusing, the intensity can also become high enough to cause strong ionization. The later is called optical breakdown. Picosecond laser induced optical break down is confirmed to have lower threshold in tap water than in distilled water [22, 24]. The reason is claimed to be the impurity(mostly alkali ions), which adds extra free electron to the water so that the free electron density in equilibrium is higher in tap water. Though the multiphoton ionization rate does not depend on free electron density, the avalanche ionization rate does. This confirmed the avalanche ionization is significant in picosecond laser matter interaction.

3.1 White Light Generation of Filamentation in Water with Impurities

Filamentation results from the interplay of Kerr self-focusing and plasma defocusing. Because the intensity dependent refractive index is almost the same in different water, the self-focusing is also the same. So if the dynamics of ionization is different in different water, the dynamics of filamentation should be different.

This assumption is tested experimentally. The white light generation is one of the signature of filamentation. So, in the experiment, the difference is studied by quantifying the white light generation in distilled water and tap water, induced by pulse of different energy. The setup is shown in Fig.3.1. Because of the high sensitivity of the output spectrum to the initial pulse condition, small defect of the water chamber can cause big spectrum shift and result in wrong conclusion. So, I machined the chamber on milling machine with 5×10^{-3} inch precision. 5 mm fused silica high-precision windows from Thorlab is used on both sides of the chamber.

The total energy of the < 750 nm component of the output pulse at different input pulse energy is measured. The result is presented in Fig.3.2. The result shows no difference between water of different purity. If water with different purity have different ionization threshold, as confirmed in[22, 24] , we should also observe difference in Fig.3.2. Because different ionization threshold corresponds to different clamping intensity. If the pulse is clampped at lower intensity, the self phase modulation effect will be weaker. Thus the spectrum will be less broadened.

One possible explanation is: Because of ultrashort pulse duration, avalanche ionization plays a negligible role in filamentation of femtosecond pulses, under our conditions.

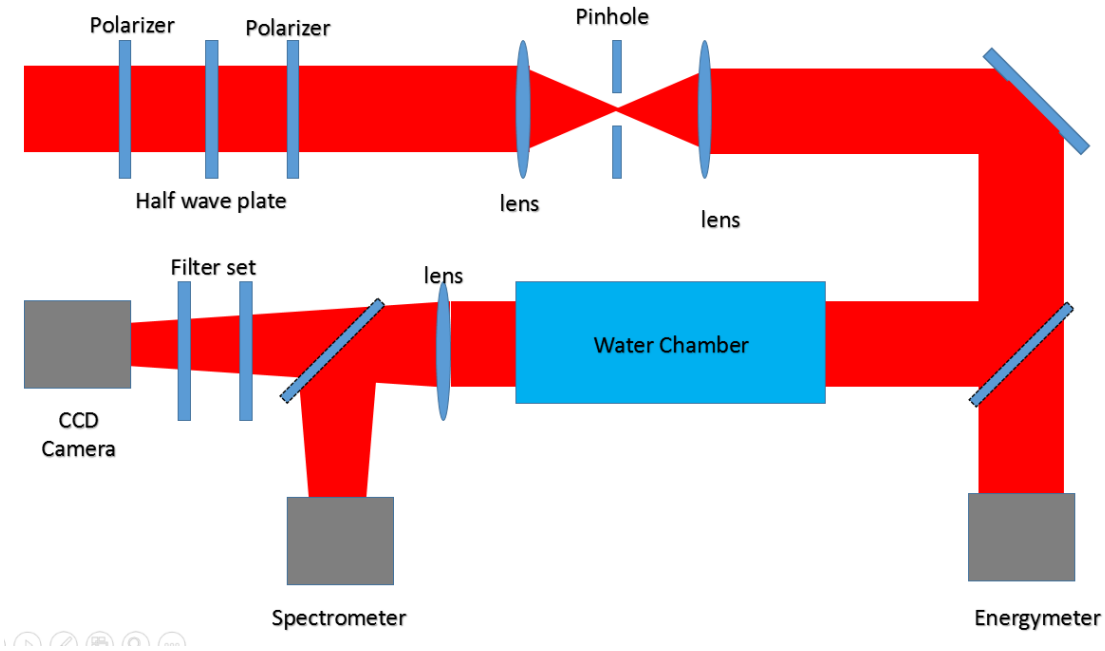

Figure 3.1: Sketch of the setup used to measure the difference between filamentation in tap water and that in distilled water. The input pulse first have its intensity adjusted and polarized passing through a set of two polarizer and a half wave plate. The spatial filter made up with two lens and a pinhole cleaned the spatial profile of the pulse. The mirror drawn in dashed line can be removed so that the energy of the pulse can be measured. After passing through the water chamber, it is loosely focused by the lens, so most of the white light generated during filamentation can be captured by the CCD camera or the spectrometer. The filter set contains a mirror that has 99% reflection for light > 750 nm and a low pass filter transmitting light < 750 nm.

Difference between water and methanol water solution (2% methanol measured in volume) is also studied. Difference in self-focusing process is still negligible, because the intensity dependent refractive index should be the weighted

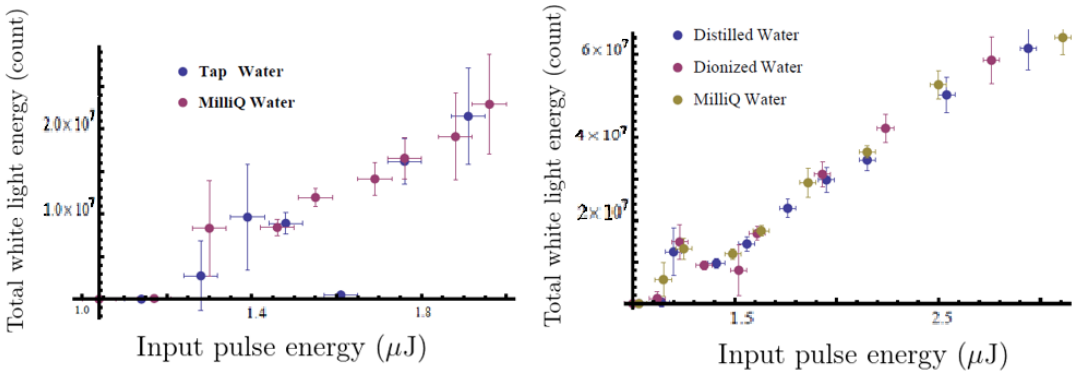

Figure 3.2: Total energy of the < 750 nm components of output pulse versus input pulse energy. This result quantifies how much does the spectrum of the input pulse is broadened through self phase modulation. (a) Is the comparison between distilled water, deionized water, and Milli-Q water. (b) is comparison between distilled water and tap water. Each measurement is averaged over at least 600 shots.

average of all component of the solution. The difference is still in the ionization process. The multiphoton absorption in water is a 5 photon process. The band gap of methanol is about 6.2 eV [3], for 800 nm light, the ratio of $E_{gap}/(h\nu)$ is about 4.03. No matter it is the 5-photon ionization or the 4-photon ionization that dominate, the multiphoton ionization is at least same likely to happen for methanol (or more likely to happen). But the threshold for avalanche ionization will be different. Because free electron need less energy to ionize another bounded electron in methanol. So, having different ionization dynamics, the white light generation in water and methanol water solution should also be different.

The experimental result of total energy of the < 750 nm component of the output pulse versus different input pulse energy is measured, and presented in Fig.3.3. No difference is observed. To further confirm it, the spectrum of output

pulse is measured at different input energy. From the spectrum measurement shown in Fig. 3.4, it is clear that the dynamics of the filamentation in water and 2% methanol water solution are almost identical. This can still be explained by the negligible role of avalanche ionization in femtosecond filmentation.

One of the very tricky parts of the experiment is that water with a small amount of methanol added can easily form colloid and greatly affect the measurement. Although methanol is commonly thought to be able to dissolve in water in any amount, it should be analytical grade. Otherwise those organic impurity dissolved in methanol will deposit during mixing. In such case, the solution will become colloid. This can be confirmed by Tyndall effect. The scattering in colloid significantly affects the measurement. Even the methanol used is analytical grade, after stored in the plastic bottle (commonly used in optic labs), it will be contaminated. Also, if the water chamber is made with plastic or aluminum, it can be easily eroded by methanol water solution. So for this part, I machined another chamber with stainless steel.

3.2 Conclusion

The dynamics of femtosecond filamentation in water is not affected by free electrons introduced by impurities. It is also not affected by adding methanol (which has lower the ionization energy). The minor role of avalanche ionization in femtosecond pulse propagation could explain the absence of difference. In order to confirm it, further theoretical work and experiments have to be done. It should also be noticed that water added with methanol can easily form a colloid thus result in wrong experiment result.

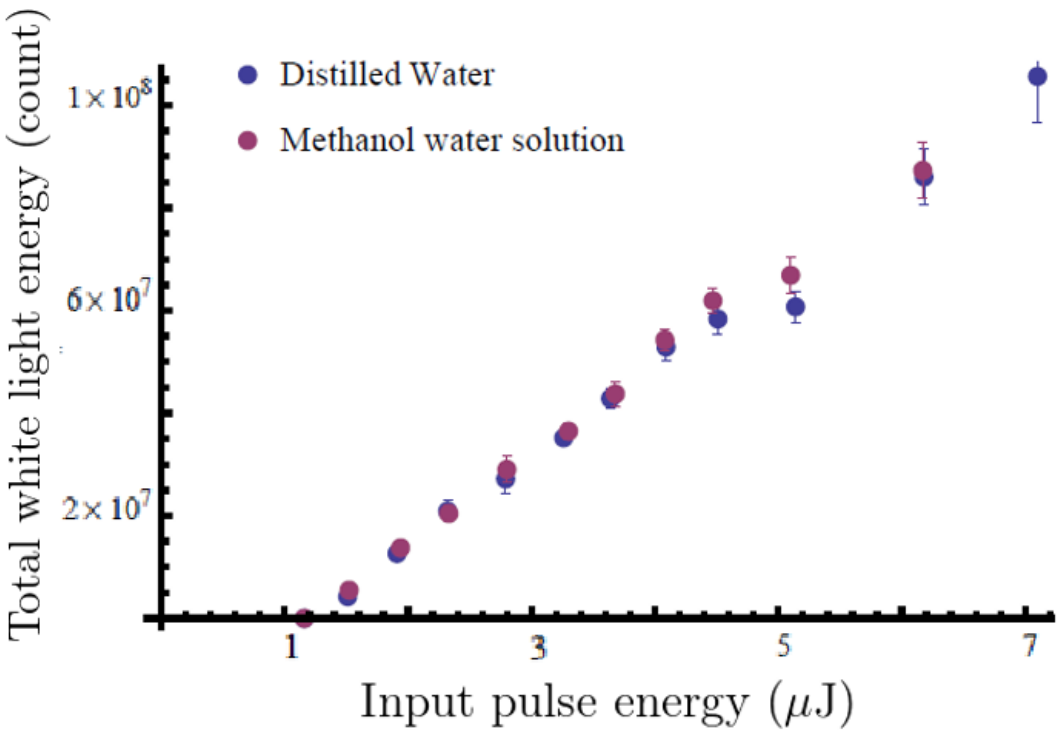

Figure 3.3: Total energy of the < 750 nm components of output pulse versus input pulse energy. This result quantifies how much the spectrum of the input pulse is broadened through self phase modulation. The two curves correspond to water and water added with methanol (4 ml methanol is added to make total volume 200 ml). Each measurement is averaged over at least 600 shots

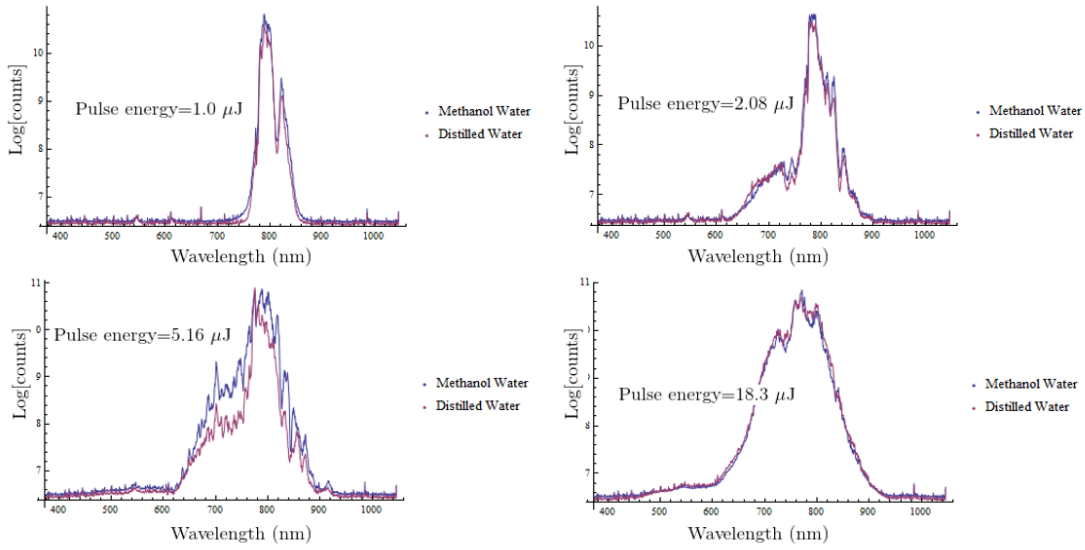

Figure 3.4: Spectrum of pulse after filamentation in water and water added with methanol (4 ml methanol and total volum 200 ml). Measurement is done with different input pulse energy(as marked in graph). Each measurement is averaged over at 300 shots.

BIBLIOGRAPHY

[1] Robert W Boyd. *Nonlinear optics*. Academic press, 2003.

[2] A Braun, G Korn, X Liu, D Du, J Squier, and G Mourou. Self-channeling of high-peak-power femtosecond laser pulses in air, 1995.

[3] A Brodeur and SL Chin. Band-gap dependence of the ultrafast white-light continuum. *Physical review letters*, 80(20):4406, 1998.

[4] Ri Y Chiao, E Garmire, and CH Townes. Self-trapping of optical beams. *Physical Review Letters*, 13(15):479, 1964.

[5] Arnaud Couairon and Andre Mysyrowicz. Femtosecond filamentation in transparent media. *Physics reports*, 441(2):47–189, 2007.

[6] Arthur Dogariu, James B Michael, Marlan O Scully, and Richard B Miles. High-gain backward lasing in air. *Science*, 331(6016):442–445, 2011.

[7] D Du, X Liu, G Korn, J Squier, and G Mourou. Laser-induced breakdown by impact ionization in sio2 with pulse widths from 7 ns to 150 fs. *Applied physics letters*, 64(23):3071–3073, 1994.

[8] CG Durfee III, J Lynch, and HM Milchberg. Development of a plasma waveguide for high-intensity laser pulses. *Physical Review E*, 51(3):2368, 1995.

[9] MD Feit and JA Fleck Jr. Effect of refraction on spot-size dependence of laser-induced breakdown. *Applied Physics Letters*, 24(4):169–172, 1974.

[10] Gadi Fibich, Shmuel Eisenmann, Boaz Ilan, Yossi Erlich, Moshe Fraenkel, Zohar Henis, Alexander Gaeta, and Arie Zigler. Self-focusing distance of very high power laser pulses. *Optics express*, 13(15):5897–5903, 2005.

[11] Gadi Fibich and Boaz Ilan. Optical light bullets in a pure kerr medium. *Optics letters*, 29(8):887–889, 2004.

[12] Alexander L Gaeta. Catastrophic collapse of ultrashort pulses. *Physical Review Letters*, 84(16):3582, 2000.

[13] Rafael R Gattass and Eric Mazur. Femtosecond laser micromachining in transparent materials. *Nature photonics*, 2(4):219–225, 2008.

[14] Taylor Grow and Alexander Gaeta. Dependence of multiple filamentation on beam ellipticity. *Optics express*, 13(12):4594–4599, 2005.

[15] Taylor D Grow, Amiel A Ishaaya, Luat T Vuong, and Alexander L Gaeta. Collapse and stability of necklace beams in kerr media. *Physical review letters*, 99(13):133902, 2007.

[16] H Maillotte, J Monneret, A Barthelemy, and C Froehly. Laser beam self-splitting into solitons by optical kerr nonlinearity. *Optics communications*, 109(3):265–271, 1994.

[17] Grégoire Méchain, Arnaud Couairon, Y-B André, Ciro DAmico, Michel Franco, Bernard Prade, Stellios Tzortzakis, André Mysyrowicz, and Roland Sauerbrey. Long-range self-channeling of infrared laser pulses in air: a new propagation regime without ionization. *Applied Physics B*, 79(3):379–382, 2004.

[18] Grégoire Méchain, Ciro DAmico, Y-B André, Stellios Tzortzakis, Michel Franco, Bernard Prade, André Mysyrowicz, Arnaud Couairon, Estelle Salmon, and Roland Sauerbrey. Range of plasma filaments created in air by a multi-terawatt femtosecond laser. *Optics Communications*, 247(1):171–180, 2005.

[19] Stefano Minardi, Carles Milián, Donatas Majus, Amrutha Gopal, Gintaras Tamošauskas, Arnaud Couairon, Thomas Pertsch, and Audrius Dubietis. Energy deposition dynamics of femtosecond pulses in water. *Applied Physics Letters*, 105(22):224104, 2014.

[20] KD Moll, Alexander L Gaeta, and Gadi Fibich. Self-similar optical wave collapse: observation of the townes profile. *Physical review letters*, 90(20):203902, 2003.

[21] Bernard Prade, Michel Franco, André Mysyrowicz, Arnaud Couairon, Helge Buersing, Bernd Eberle, Marcel Krenz, Dirk Seiffer, and Olivier Vasseur. Spatial mode cleaning by femtosecond filamentation in air. *Optics letters*, 31(17):2601–2603, 2006.

[22] CA Sacchi. Laser-induced electric breakdown in water. *JOSA B*, 8(2):337–345, 1991.

[23] Marin Soljačić, Suzanne Sears, and Mordechai Segev. Self-trapping of necklace beams in self-focusing kerr media. *Physical review letters*, 81(22):4851, 1998.

[24] Alexander M Streltsov and Nicholas F Borrelli. Study of femtosecond-laser-written waveguides in glasses. *JOSA B*, 19(10):2496–2504, 2002.

[25] H Wille, Miguel Rodríguez, Jérôme Kasparian, Didier Mondelain, Jin Yu, André Mysyrowicz, Roland Sauerbrey, Jean-Pierre Wolf, and Ludger Woeste. Teramobile: A mobile femtosecond-terawatt laser and detection system. *The European Physical Journal Applied Physics*, 20(03):183–190, 2002.

[26] Ji Zhonggang, Zhu Jiabin, Wang Zhanxin, Ge Xiaochun, Wang Wenyue, Liu Jiansheng, and Li Ruxin. Low resistance and long lifetime plasma channel generated by filamentation of femtosecond laser pulses in air. *Plasma Science and Technology*, 12(3):295, 2010.